Eidgenössische Technische Hochschule Zürich
Swiss Federal Institute of Technology Zurich

Semester Thesis

Realization of an Active Magnetic Field Compensation

Author:
Valentin Goblot

Supervisor:
Tobias Thiele

Professor:
Prof. Andreas Wallraff

September 10, 2014

Abstract

Ambient magnetic fields are the cause for a deflection of the electron beam in the Rydberg Experiment in the Quantum Device Lab, degrading the quality of measurements. In order to prevent this effect, a set of coils was built and an active compensation of the magnetic field at the experimental setup was realized. The coils were designed such that they fit around the experiment and compensation of $\sim 100\mu$T ambient fields was reached with current less than 1A per coil. It is shown that the deflection of the electron beam can be tuned by adjusting the currents in the coils, until the effective magnetic field orthogonal to the beam propagation axis reaches a zero value. The quality of the Rydberg spectra is increased when compensation is present, and more precise characterizations of the beam are made possible.

Contents

1 Theoretical study of the coils setup

Because of their long coherence times, Rydberg atoms are interesting for quantum information and could be used in hybrid quantum systems as a mean of information storage. The Rydberg experiment in the Quantum device lab aims to couple Rydberg atoms and superconducting circuits [1]. The experimental setup consists of a supersonic beam of $1s^1\ 2s^1\ ^1S_0$ He atoms that are prepared in a np Rydberg state, typically $n \approx 30$, and pass close to a superconducting surface. He Rydberg atoms are then ionized and the resulting electrons are measured by a microchannel plate (MCP) after propagating over a distance $D \approx 15$cm.

1.1 Presentation of the problem

An earlier study [2] has found that parasitic magnetic fields created by magnets in neighbouring labs have a significant impact on the experiment via two effects: deflection of the electron beam between the ionization region and the detection region, and the motional Stark effect. In the present work we focus on the electron deflection problem. We can thus restrict the system to a simple model of an electron beam propagating in free space along the z direction, under the influence of a magnetic field. The beam is deflected because of the Lorentz force that acts on the electrons. The amplitude of ambient magnetic fields in the lab varies with time, and can reach values such that the deflection of the electron beam is bigger than the size of the MCP, with the result of a significant part of the electrons not being detected, degrading the measurements quality.

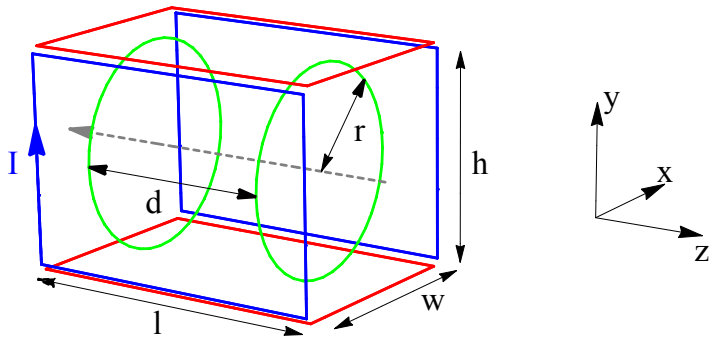

Figure 1: Schematic coils configuration. The origin of coordinates $(0, 0, 0)$ is at the center of each coil pair. The dashed gray arrow represents the electron beam. The blue arrow indicates the convention for positive intensity.

The earlier study has suggested to address the problem using an active shielding compensation of three pairs of coils, one pair having as main axis its own direction of space. The configuration used in this work is represented in Fig. 1. A circular pair of coils was chosen for the beam propagation axis (z-axis) because circular coils fit better around the vacuum chamber in which the He atoms and electrons propagate. Moreover, they can be brought in Helmholtz configuration, providing better magnetic field homogeneity. Note also that the center of the coils setup is chosen to match with the region where electrons are generated from He atoms in the experiment.

1.2 Coils design

In order to determine the optimal design of the coils, simulations of the magnetic field that can be generated have been done. An approximate value of the field $\vec{B}$ produced by a current I flowing through a rectangular coil consisting of N windings can be calculated from Biot-Savart's law linking magnetic field and current density: see Appendix A and [3] for the full derivation.

$$\vec{B}(\vec{r}) = \frac{\mu_0}{4\pi} NI \oint \frac{d\vec{l} \times \vec{r'}}{r'^3} \tag{1.1}$$

For circular coils, the derivation is slightly different and starts with the evaluation of the vector potential [4]. Considering a single coil, e.g coil $Z1$ with center position $(0, 0, d/2)$, in cylindrical coordinates:

$$\vec{B}(\rho, z) = (B_\rho, B_\phi, B_z) \quad , \tag{1.2}$$

the final expressions are:

$$B_\rho(\rho, z) = -\frac{\mu_0}{4\pi} NI.(z - d/2) \frac{k}{\rho\sqrt{r\rho}} \left(K(k) - \frac{2 - k^2}{2(1 - k^2)} E(k) \right) \tag{1.3}$$

$$B_\phi(\rho, z) = 0 \tag{1.4}$$

$$B_z(\rho, z) = -\frac{\mu_0}{4\pi} NI \frac{k}{\sqrt{r\rho}} \left(K(k) + \frac{k^2(r + \rho) - 2\rho}{2\rho(1 - k^2)} E(k) \right) \tag{1.5}$$

where k is given by

$$k = \sqrt{\frac{4r\rho}{(r + \rho)^2 + (z - d/2)^2}} \tag{1.6}$$

and $K(k)$ and $E(k)$ are the complete elliptic integrals of the first and second kind, respectively. The magnetic field density $\vec{B}_{Z2}$ created by the second circular coil is obtained by changing $d/2$ to $-d/2$ in (1.3), (1.4), (1.5) and (1.6).

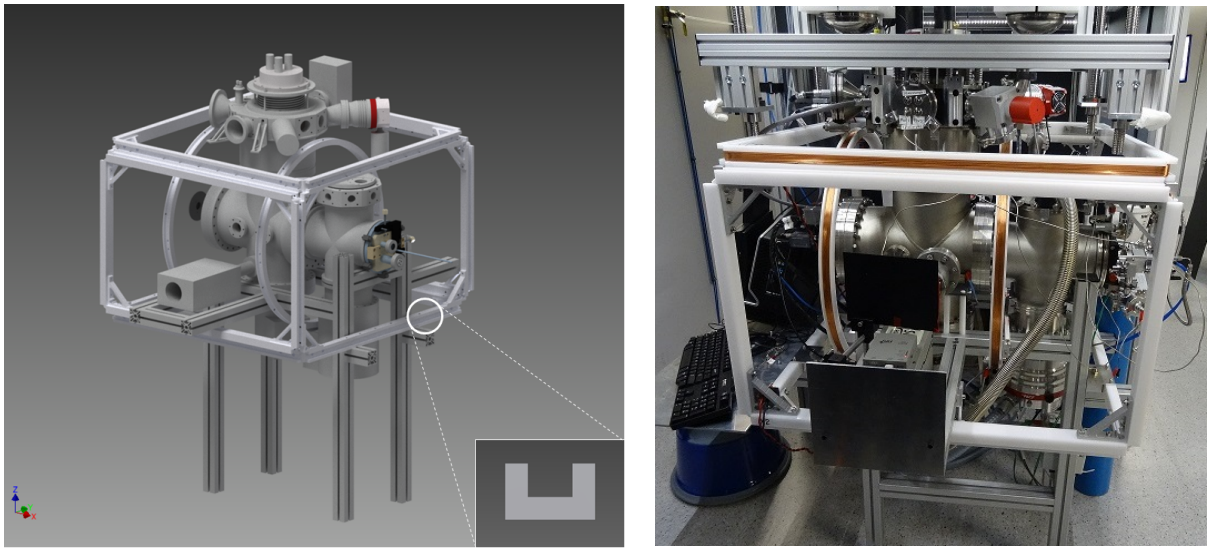

Figure 2: Left: Simulation of how coils with the final dimensions, see Table 1, fit around the experimental setup. Only the U-shaped profiles (see inset) of the coils structure, that carry the copper wire, are represented (see section 2.1). Right: Picture of the final coils around the experimental setup.

We are mainly interested in the field produced along the beam propagation axis, i.e z-axis. The goal is to be able to compensate the ambient magnetic field as good as possible on the whole electron path. Along this axis, the field produced by rectangular coils will be more homogeneous if the coils are bigger. Therefore, big rectangular coils will produce a big and homogeneous compensated region, the tradeoff being the need for a higher intensity factor NI to produce a magnetic field. The same argument is also valid for circular coils. Moreover, circular coils are more efficient and the fields more homogeneous when they are placed in Helmholtz configuration, where the distance between them is such that $d = r$, see Fig. 1. However, the main problem for dimensioning the coils is to fit them around the experiment. Indeed, the complexity of the experimental setup configuration only lets a small room for manoeuvre. Thus, we choose the coils dimension parameters such that it fits well, taking the previous remarks into account as much as possible. For example, the radius of the circular coils can only be chosen in a range of 30 ± 2 cm. The Helmholtz configuration is thus not accessible currently, see Fig. 2, but will be if the experiment is extended with the new helium source [5, 6]. The final dimensions of the coils are given in Table 1, Fig. 2 presents a simulation of the final setup.

Parameter	Value (cm)
w	80
h	50
l	80
r	30
d	40

Table 1: Final dimensions of the coils, using the notations from Fig. 1.

1.3 Simulation of the compensation

There is still a degree of freedom that needs to be chosen for optimized fields produced by our coils: the proportionality factor NI, or equivalently the number of windings per coil N. The criteria for the determination of this parameters is to be able to compensate the ambient field given the available power to feed the coils. The device providing current to the coils is described in [2]. Given the characteristics of this device, we want to restrict the current in the coils to a maximum of 1A. We use the design and calculations from the last section to simulate the field produced by the coils setup and adjust the proportionality factor NI of each coil such that a given ambient magnetic field is compensated along the propagation of the electron beam. From the upper bound on available intensity we obtain a lower bound for winding number. Two cases are considered for the ambient magnetic field to compensate: a uniform magnetic field and a gradient field.

For the first case, considering the measured range for the value of the ambient magnetic field in the lab [2], we consider a worst case scenario of an ambient uniform field of 200μT, with a random direction. To compensate for a uniform field, it is sufficient to use the same current for the two coils of a pair, letting only three parameters to determine: NI_X, NI_Y and NI_Z. The criteria for the compensation is to have an amplitude of 0 in the center of the coils, i.e in position $(0, 0, 0)$. For a given field direction, we have a linear system of three equation with three unknowns, that we solve to find the required currents. The simulation results are presented Fig. 3. We define the *compensation region* as the region in which the field amplitude is less than 10% of the ambient field, i.e in this case 20μT. The origin of the electron beam, i.e. the ionization region matches the center of the coils and the other end of the electron path is the MCP, which sits at the end of the vacuum chamber, approximately at the position of coil Z2 and 15cm away from the ionization region. The compensation region has to cover the whole electron path to be in a good compensation situation. This is

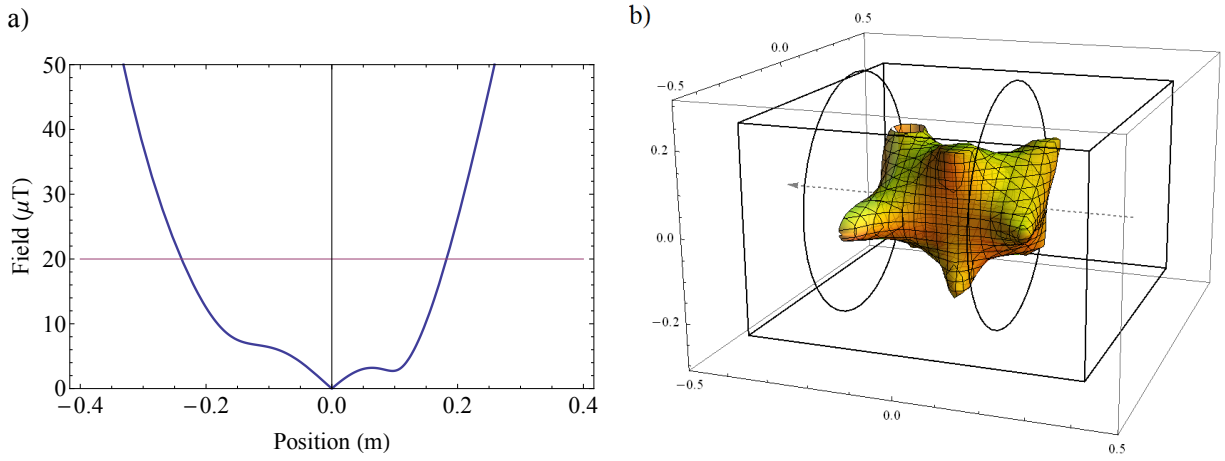

Figure 3: Simulation results for the compensation of a uniform ambient field. (a) Compensated field along the beam propagation axis. The thin red line represents 10% of the ambient field, i.e the definition of the boundaries of the compensation region. The currents were adjusted so that the field is perfectly zero in the centre of the coils. (b) Full compensation region with the same currents. The black lines represent the coils configuration, the dashed gray arrow is the electron path. The electrons are actually generated in $(0, 0, 0)$ and the MCP is approximately at the position of the left circular coil, on z axis.

the case in Fig. 3.b, which is a validation of the coils setup design. Such a simulation was repeated with different direction for the ambient field to refine the condition on winding number required. In the end, every field of 200μT can be perfectly compensated in the center of the coils, with an acceptable compensation region extent and with less than 1A flowing through each coil, provided that $N > 150$.

For the gradient field simulation, we start from the field measured in two positions around the experimental setup in the lab. From there on, we extrapolate to define the ambient field. This time, different currents are used in each coil, and the criteria for the compensation is a zero amplitude of the field in two positions along the z axis, or at least close to the z axis since the equation system might be of a rank smaller than 6 if the two points are chosen perfectly on the axis. The results of such a simulation are presented Fig. 4. Note that two measurement positions are not enough to fully determine a gradient field, and we can choose between several models of dependance in coordinates (x, y, z) in the extrapolation. Running simulations for different models, it turns out that the compensation of a gradient field can require a higher current than in the uniform case, thus the final choice for the winding

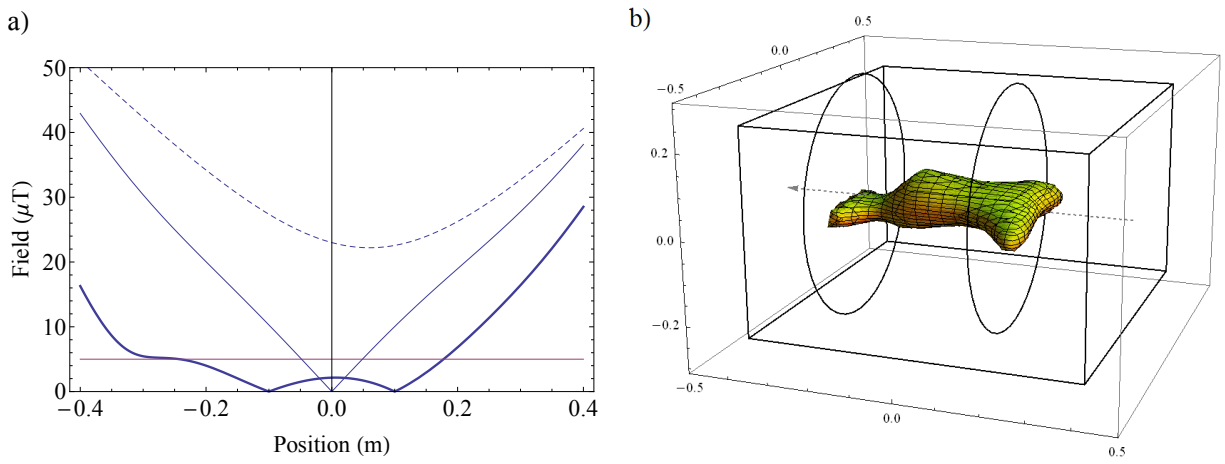

Figure 4: Simulation results for the compensation of a gradient field. (a) Compensated field along the beam propagation axis. The dashed blue line is the gradient field. The thin red line represents an arbitrary value of 5μT chosen as condition for compensation region boundaries. The thin blue line is the field when the compensation should only occur in the center. The thick blue line shows the field with currents adjusted so that the zero values are at $z = \pm 10$cm. (b) Full compensation region with the currents configuration used to get the optimal compensation as in (a).

number is $N = 200$. We choose to use the same number of windings for each coils for simplicity reasons.

2 Characterization of the coils setup

2.1 Construction of the coils

The six coils were built based on the results from the simulations carried out earlier, with dimensions given in Table 1 and a winding number $N = 200$. For the coils structure, a U-shaped profile made of Polyoxymethylene (POM) was used, as displayed in Fig. 2. For the rectangular coils, four edges of such a profile are assembled together, whereas for the circular coils two semi-circles are used. A copper wire is then wound around the structure to get the final coil. POM was chosen because it has the advantage of being reasonably light but robust at the same time, and has no magnetic properties. The copper wire used is normally isolated copper wire, with a diameter ∅0.5mm. Choosing a small diameter has the advantage of limiting the weight of copper needed, thus limiting both the need for a very robust structure to carry the coils, and the price. The negative aspect of a small diameter is high electric resistance. The values for the resistance of coils from pair X, Y and Z are $\approx 50\Omega$, $\approx 60\Omega$ and $\approx 35\Omega$.

In order to check the field that the coils produce, a measurement of the magnetic field was done. For each pair of coils, a current of 300mA was sent to each coil and the magnetic field was measured along the main direction. Only the component of the field corresponding to the main axis was measured, for example for the circular pair the measured quantity is $B_z(0, 0, z)$. The results are presented in Fig. 5 and show good agreement with theory.

2.2 Experimental compensation of magnetic fields

The coils were then installed around the experiment. From there on, the procedure used for the active compensation of ambient magnetic field is the one described in [2], including the amplifier and the feedback program. The principle of the feedback is the following: two sensors measure the magnetic field inside the region of compensation. Based on the measured values, the intensities through each coil are adjusted such that the field at the sensors come closer to the desired value. It is important to notice that although the desired value is zero along the electron beam path in the center of the compensation region, in the actual case sensors cannot be placed in this region because it is inside the vacuum chamber. Both sensors have to be placed outside the vacuum chamber, and thus the magnetic field amplitude at their position does not need to be zero in general. The final sensors positions are $S_1 = (10, 10, -15)$ and $S_2 = (-10, -10, 5)$, with coordinates in cm.

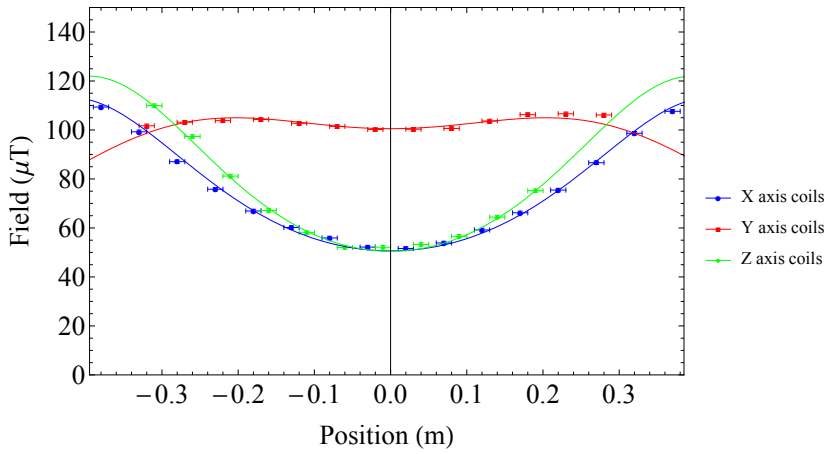

Figure 5: Magnetic field generated by each coils pair along its main axis. A current of 300mA was used in both coils of a pair, each pair being measured separately. The rectangular coils were placed in the configuration described in Table 1, whereas the circular coils were separated by 80cm for this measurement.

Another important point is the conversion from sensor signal to intensities in the coils. In the version of the feedback program used in the previous study, each coil is only driven by one component of the field which is being measured by one sensor. For example, intensity I_{X1} in coil $X1$ is fully determined by $B_X(S_1)$, I_{X2} by $B_X(S_2)$, etc. In theory, the relation between intensities in coils and magnetic fields at S_1, S_2 is linear and there is a unique solution to the compensation problem. However, in practice this way is not optimal at all because it neglects the fact that current in coil $X1$ also impacts $B_X(S_2)$, and coils might end up "fighting" each other to adjust the field to the desired value. Thus, the problem is that the compensation might not be able to reach the desired solution and tries to send a lot of current through the coils.

2.3 Cross-talk between coils

In order to improve the conversion from sensor signals to currents in coils, the influence of each coil on the field at both sensors needs to be addressed. The fact that each of the six coils influences each of the six sensor signals (three component for both sensor) is referred to as *coupling* between the coils. The knowledge of this coupling will give the full system of equations for the real coils system, allowing for better characterization, comparison to the simulated configuration and ultimately optimization of the currents sent through the coils during compensation. The measurement of the coupling

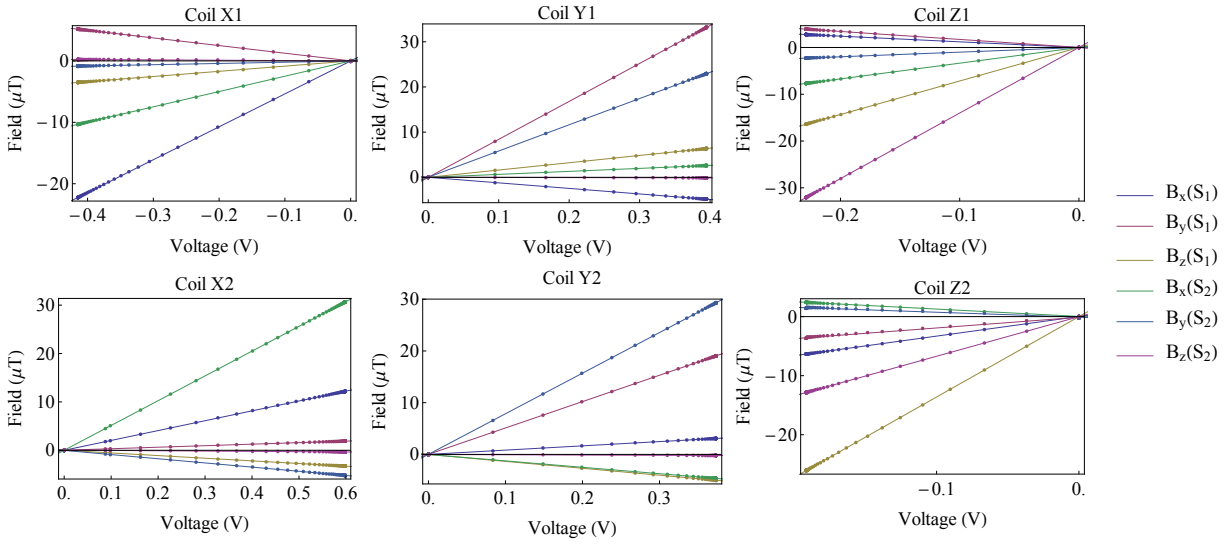

Figure 6: Field created depending on current flowing through a coil, i.e measurement of the coupling for each coil. For a given coil measurement, a residual current of 40mA was sent through all other coils to take into account some nonlinearities. The voltage parameter is the voltage sent by the input card to the amplifier.

is done by sending a defined current through a given coil and measuring the evolution of the six sensors signal. One gets a relation between current and magnetic field produced by this coil. The measurement is then repeated for the five remaining coils, as presented in Fig. 6. Note that we don't use intensities in coils as parameter but instead voltages sent by the input card that drives the amplifier. There is a conversion factor of 4/10 from the voltages in V to intensities in the coils in A. In theory, the magnetic field produced by the coils evolves linearly with the current in each coil, and we can use a vector representation for the six sensors signals and the six currents. Noting B the 6-vector magnetic field and I the 6-vector current, we can define a coupling matrix M such that:

$$B = M.I \tag{2.1}$$

where by convention I is expressed in A and B in μT. The coefficients of M are simply given by the measurement of Fig. 6, since by definition i-th column of M is the six field components measured by both sensors when 1A is sent through coil i, i.e i-th column is given by the slopes obtained for coil i in Fig. 6. Equation (2.1) enables to deduce the field measured by the sensors with the knowledge of the currents (Fig. 7), but it can also be

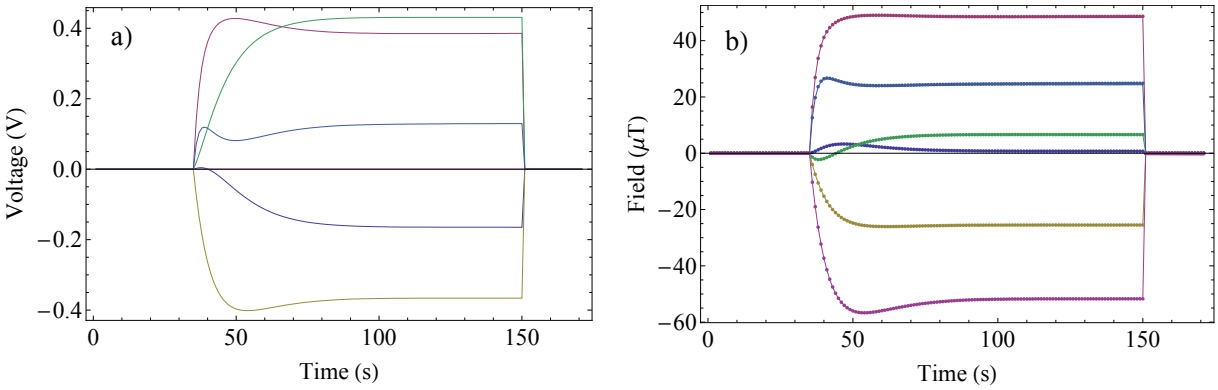

Figure 7: Reconstruction of magnetic field based on currents sent through the coils, using the coupling matrix. (a) Sequence of currents sent through the coils over a given period of time. (b) Resulting magnetic fields. Dots are the values obtained from equation (2.1), solid lines are measured values. There is a good match between expected and measured values.

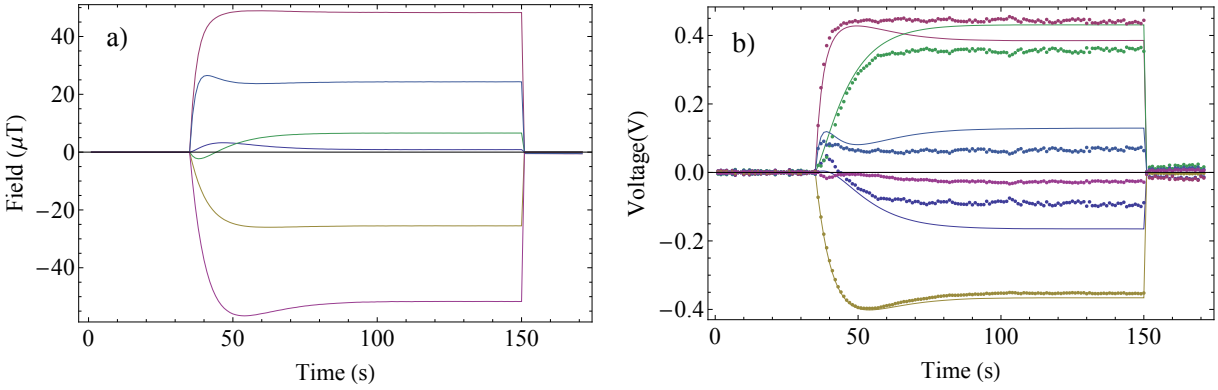

Figure 8: Inverse reconstruction of current sent through the coils based on the measured magnetic fields, using the inverted coupling matrix. (a) Same sequence of measured magnetic fields over a given period of time as in Fig. 7.b. (b) Resulting currents used to produce such fields. Dots are the values obtained from inverting equation (2.1), solid lines represent the values of the voltages sent to the input card. The match is poorer than before, indicating an error in the inversion of M, or a discrepancy between values sent to the input card and currents flowing through coils, because of, for example, non linear effects.

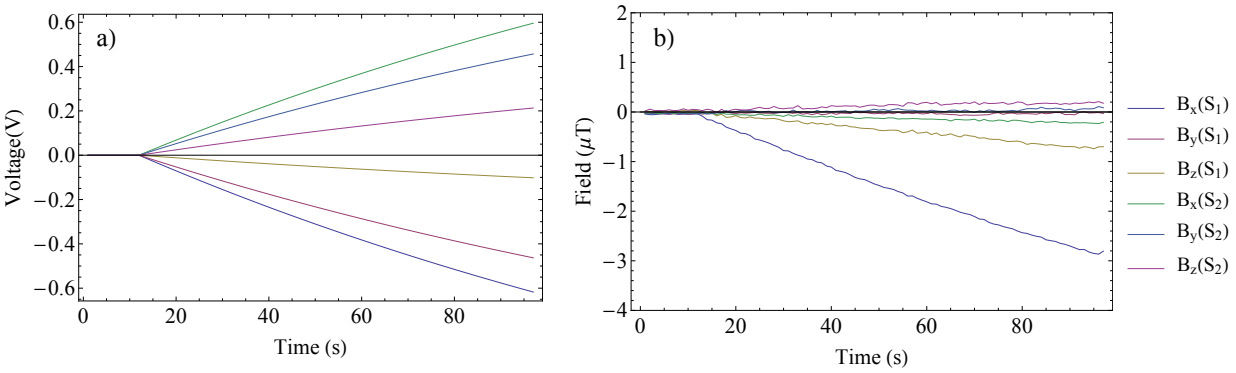

Figure 9: Drive of a single sensor signal using the inverted coupling matrix. (a) Sequence of voltages sent through the coils. (b) Resulting magnetic fields measured by the two sensors. The signal that is driven is $B_x(S_1)$, but others are slightly modified, for example $B_z(S_1)$, which is due to the error in M^{-1} already observed Fig. 8. Moreover the required currents to produce a variation of about 5μT are very important in this case.

inverted to deduce the currents in the coils given the sensors signals (Fig. 8). Fig. 7 shows a good fidelity but with a few discrepancies, indicating that the real system is not perfectly linear. Indeed, every coil shares the same current source and we observe that for a given voltage in the input card, the actual current in a coil will be lower when several other coils are also fed with current than when no other coil is used. These nonlinear features are more obvious in Fig. 8 because the inverted system is very sensible to small changes, which explains the discrepancies in the reconstruction of intensities given the sensor values.

Inverting equation (2.1) does, in theory, also enable to determine the exact currents needed to create a given set of values for the field measured by sensors. This could be used to adjust instantly the values of the field at the sensor positions, with no need for a feedback as it exists now. Another possibility is to use the inverse of M to avoid any crosstalk and be able to tune each sensor signal independently. The coupling matrix was implemented in the feedback program and Fig. 9 shows the result of trying to tune only one signal. Such a drive was achieved for small field amplitudes but the required current increases very fast and the limits on the supply makes it impossible to create a field of more than 5μT without affecting other sensor signals. Moreover, the relatively high uncertainty on M an the nonlinear features have a huge impact on the matrix inversion, resulting in some remaining coupling to other signals. For other signals it can even turn out to be impossible to tune them independently from the others. Finally, even in the case where the

independent response to each sensor signal could be achieved, this would still be far from optimal because we need to send current through the coils to make sure that only one component of the measured field is changed, i.e we have to use current to avoid creating a field, which can be very current consuming. A possibility to improve the efficiency of the drive of the coils would be using the coupling matrix to maximize the field created with minimal currents, sending more current in the coils that have the biggest influence on a given signal.

2.4 Power supply issues

During the coils characterization experiments, we noticed that the current in the coils seemed to be limited to much less than the expected 1A. Indeed, a threshold was observed for input voltages above which the magnetic field generated by the coils does not increase any further (Fig. 10). Because of this, the range of ambient field that we could compensate is heavily reduced. The threshold varies for each coil but is similar for two coils of a pair. The cause for this threshold is that since our coils have a high resistance of $\sim 50\Omega$, the voltage needed to have a current flowing through them is higher than in [2] where coils used had a resistance of $\sim 2\Omega$. As a result, the op-amps reach their saturation regime of $\pm$15V. Taking into account the transistors (see [2] for PCB design), the maximum voltage across a coil is limited to $\sim \pm$12V, which is consistent with the observed threshold values. The high resistance of the coils has also an impact in the power needed, which goes in RI^2. This is low enough to avoid cooling the coils but it can damage the components of the amplifier. Reducing the resistance of the coils is not an option, because we need to keep a high winding number, and because a thicker coil would be heavier, more expensive, and moreover we would have to wind some 3km of wire again. The solution is thus to use op-amps which work with supply voltage of $\pm$45V [7] and choose the current source such that they can also go up to 45V in voltage. This way, almost 1A should be accessible for every coil. All the op-amps where replaced eventually.

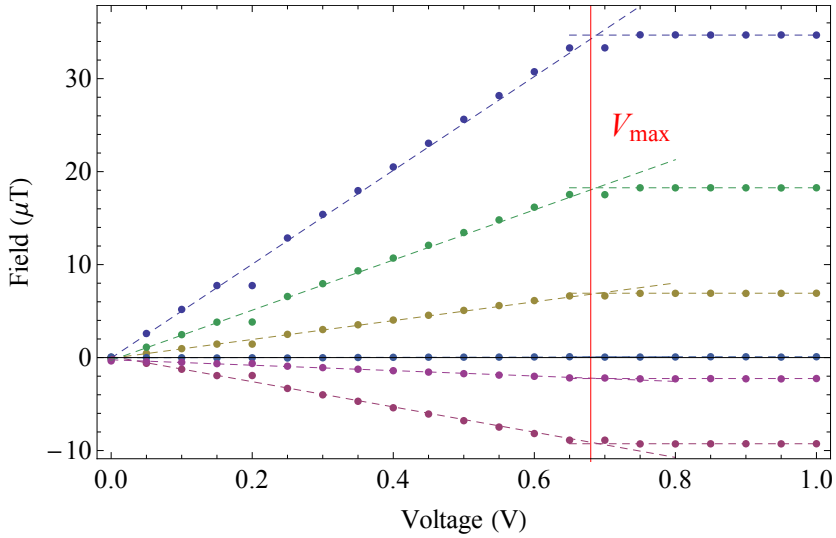

Figure 10: Threshold measurement for coil X1. For input voltage values of more than $V_{max} = 0.68$V, the magnetic field generated no longer increases, indicating a maximum available intensity from current sources $I_{X1,max} = 270$mA. A similar phenomenon is observed for negative currents and for each coil.

3 Results of the compensation

3.1 Correction of the electron beam deviation

The characterization of the coils allows us to have a good knowledge of the magnetic field produced and enables a good adjustment of the field at the sensors position. However, since the sensors are relatively far from the electron path, knowing the field value at their position is not sufficient to ensure a good compensation along the beam propagation. For example, adjusting the sensors signal to zero in x or y direction would lead to a value of 5 to 10 μT in the center of the coils. We thus need to define a procedure to reach optimal compensation. In the following, we use the imaging provided by a camera placed behind the phosphor screen of the MCP to detect the electrons arrival position and measure the beam deviation (Fig. 11). We refer to this imaging device as the MCP screen.

The deflection of an electron propagating in a magnetic field is due to the Lorentz force:

$$\vec{F} = m \cdot \ddot{\vec{x}} = -\, e \cdot \vec{v} \times \vec{B} \tag{3.1}$$

where $\vec{F}$ is the force that acts on the electron, $\ddot{\vec{x}}$ the electron acceleration, m its mass, e its charge and $\vec{v}$ its speed. We notice that only the components of the field orthogonal to the propagation direction have an influence on the deviation. Moreover, component B_y is responsible for a deviation along x

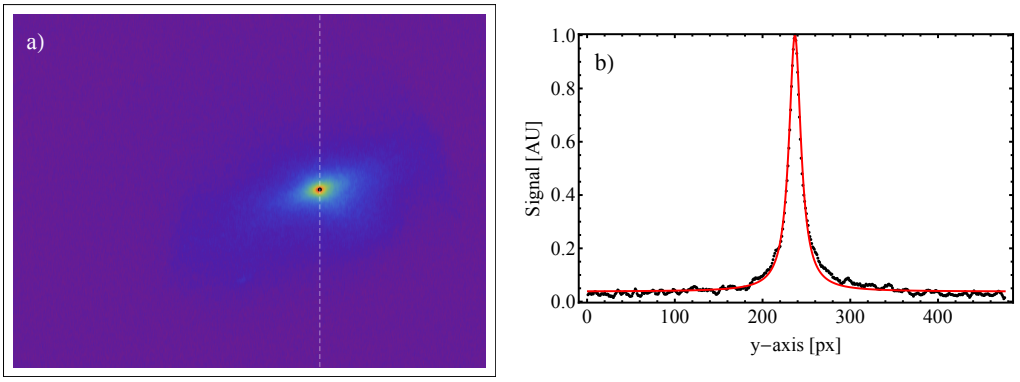

Figure 11: (a) Example of a picture captured on the MCP screen. The bright region corresponds to the high electron signal, i.e. the electron beam cross-section. The Black dot is the fitted center position of the beam determined by a lorentzian fit. (b) Intensity profile along the vertical dashed line in (a). The red line is the fitted lorentzian function, used to determine the y coordinate of the beam center position. The same is done along a horizontal line to determine the x coordinate of the center.

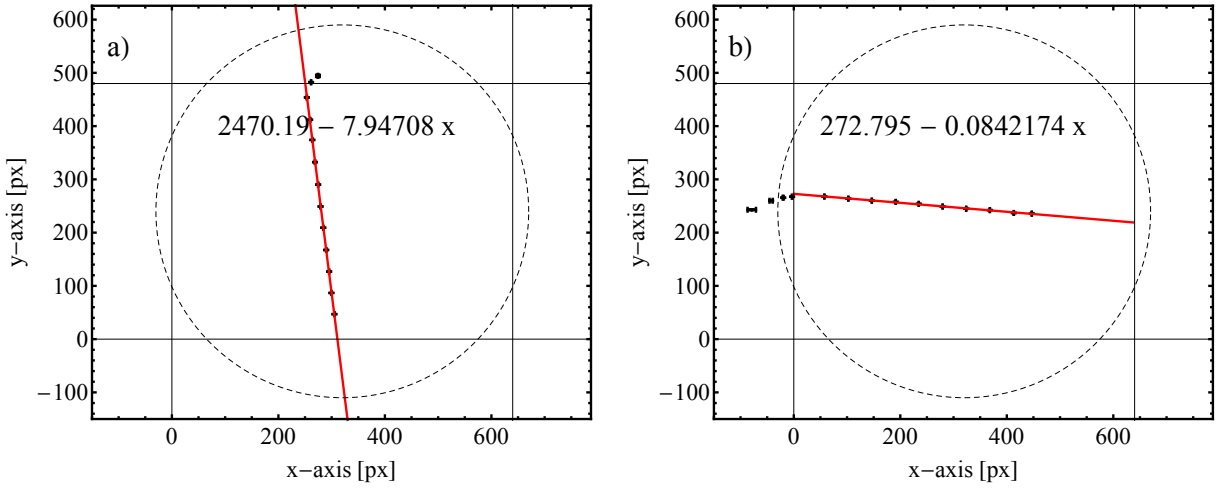

Figure 12: Influence of the magnetic field on the electron beam deviation. (a) B_x was tuned while B_y was kept constant. (b) B_y was tuned while B_x was kept constant. The dots correspond to the fitted beam center, using a lorentzian fit for the beam shape (Fig. 11). The points that are not aligned correspond to deviations such that a part of the beam miss the MCP, leading to spurious detection of the beam center position. The black lines indicate the extremities of the camera screen and dashed circle the boundaries of the MCP.

axis. A solution to reach optimal compensation would be to tune B_y such that the electrons are not deflected in the x direction, and do the same for B_x such that they hit the center of the MCP. This effect was thus measured by tuning the desired B_y value of both sensors and detecting the arrival position of the electron beam on the MCP. The same was done for component B_x. The results are presented in Fig. 12.

Tuning B_y, we notice that we don't get a horizontal slope as expected. This indicates that the MCP might not be perfectly aligned with our axes. In other words, we would need to calibrate the detection on the MCP such that we can identify the x and y axes direction on the MCP screen. This is also true for the center of the MCP: since we cannot ascertain that the MCP is perfectly aligned with the electron beam, we cannot determine precisely where the theoretical point of arrival of non-deflected electrons is on the screen. It does certainly not correspond to the center of the screen and thus this is not an intrinsic method to determine the optimal compensation. The good point however, is that we are successfully able to tune the beam deviation to any point on the screen.

3.2 Influence of Rydberg atoms state number on electron beam deviation

An important parameter for Rydberg atoms is the quantum number of the np state in which they are prepared. In the experiment, this is determined directly by the wavelength of the tunable excitation laser. If we develop further the expression of the electron beam deviation starting from equation (3.1), we find that the electron deviation depends on n. Indeed, under the approximation that $\vec{v}$ is constant, which remains valid for short propagation times, equation (3.1) results in a transverse deviation [2]

$$\Delta x(D) = -\frac{e \cdot D^2}{2m} \cdot \frac{B}{v} \tag{3.2}$$

where we considered a magnetic field $\vec{B}$ orthogonal to the electron propagation direction and where D is the distance the electron travels under the influence of the magnetic field (Fig. 13). We find that the electron speed depends on the np state in which He atoms are when they are ionized, by first equating the electron kinetic energy and the potential energy due to the ionization field:

$$F = eU = \frac{1}{2}mv^2 \tag{3.3}$$

In the experiment the ionization voltage U is set to 1.2kV to ensure ionization regardless of the n state. However, a pulsed ionization voltage is used, which ramps up in approximately 40ns. As a result, the electric field also ramps up from zero to the maximum value, and He atoms are ionized as soon as the their ionization field value is reached. For Rydberg atoms, the classical ionization field has a dependance $F \propto n^{-4}$. Inserting this result in (3.3) and (3.2) we obtain:

$$\Delta x \propto n^2 \tag{3.4}$$

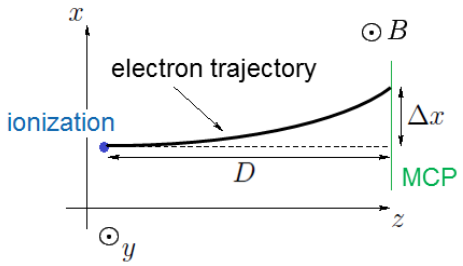

Figure 13: Simplified picture of the electron beam deflected by a magnetic field.

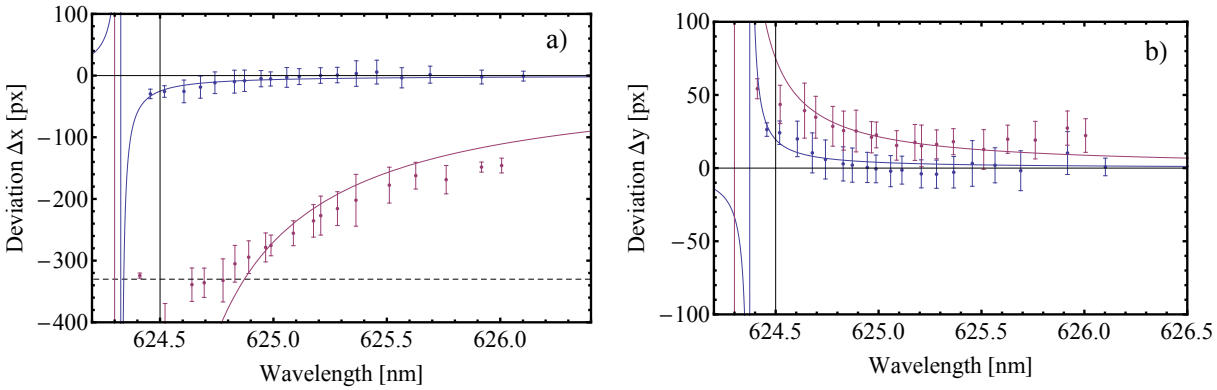

Figure 14: Electron beam deviation depending on the excitation laser wavelength, which is equivalent to np state number. (a) Deviation in the x direction. (b) Deviation in the y direction. The purple dots are without a magnetic field compensation, the blue dots are with an optimal compensation as described in section 3.3. The solid lines correspond to the theoretical formula (3.6), with fitted proportionality constant. The dashed line is the extremity of the MCP. For lower n, i.e higher λ, the low peak intensity makes the error bars bigger, which is not taken into consideration here.

Equation (3.4) describes the deviation as a function of the quantum number. This dependence was measured by detecting the beam position on the MCP for different values of the excitation laser's wavelength, at a fixed magnetic field, both without and with a magnetic field compensation. In Fig. 14, deviations in the x and y directions are plotted against the excitation wavelength λ. The theoretical lines can be obtained from (3.4), using the equality between excitation photon energy and Rydberg atom energy:

$$E_n = E_\infty - \frac{R}{n^2} = h\frac{c}{\lambda_e} \tag{3.5}$$

where R is the Rydberg energy and E_∞ corresponds to the ionization energy of our Rydberg atoms. Since a frequency doubler is used, the excitation photon wavelength λ_e is twice smaller than the tunable laser wavelength. As a result, we get:

$$\Delta x \propto \left(\frac{1}{\lambda_0} - \frac{1}{\lambda}\right) \tag{3.6}$$

with λ_0 being the ionization laser wavelength. The theoretical value for $1s^1\ 2s^1\ {}^1S_0$ He atom is 624.37nm.

Thus, we have a new criteria in the definition of an optimal compensation: the electron beam deviation on the MCP has to be zero whatever the np

state is. This effect can be used in our advantage to define a procedure for an optimal compensation.

3.3 Procedure for optimal compensation

We notice that lower np states are less deflected by a given magnetic field, and we are going to use this to reach an optimal compensation. We start with no compensation at all and select two state numbers: a low n_l and a high n_h, with $n_l < n_h$, or equivalently two laser wavelengths λ_l and λ_h (note that $\lambda_l > \lambda_h$). We then iterate the following steps:

- Set the laser frequency to λ_l to prepare atoms in low n_l state.
- Mark the arrival position on the MCP of the beam corresponding to low n_l state.
- Set the laser frequency to λ_h to prepare atoms in high n_h state.
- Tune components B_x and B_y such that the beam position for n_h state matches with the position of n_l state previously marked

When we set the laser frequency to λ_l again, the arrival position of the beam corresponding to low n_l state beam has changed, because the magnetic field was changed. However, the difference of positions decreases at each iteration, and the change of field required to match the position of n_h state becomes smaller. Whenever the new position of n_l state matches the one from the previous step, the iteration ends. When tuning B_x and B_y, one should first adjust to the same value for both sensors, and in a second time play on each sensor individually to account for gradient fields. As an example, this procedure was used choosing $\lambda_l = 626.32$nm and $\lambda_h = 624.946$nm.

Note that this procedure does not give indication on B_z compensation with Z coils. In theory B_z should not have any influence on the electrons deflection, but it is still preferable to compensate for to avoid any other possible effect. One solution is to adjust the sensors signal for B_z to zero or as close as possible given available power from the sources.

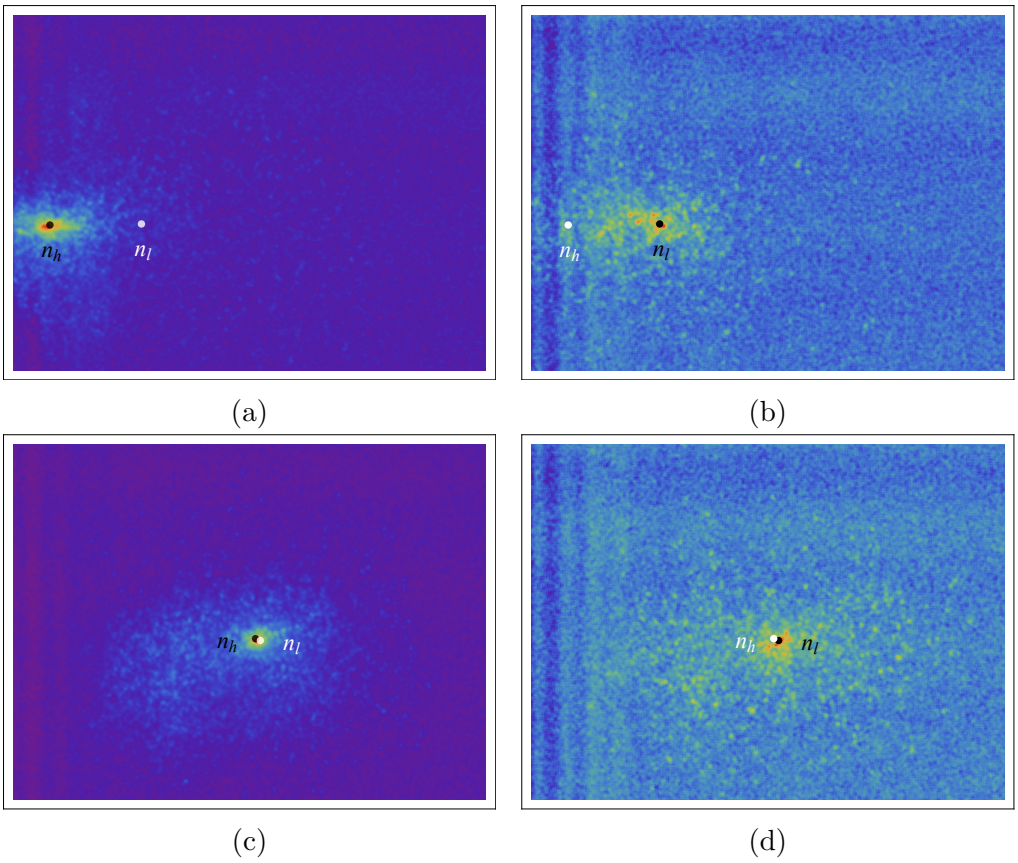

Figure 15: Pictures of the deflected electron beam detection on the MCP. (a) High n_h state, without magnetic field compensation. (b) Low n_l state, without compensation. (c) High n_h state, with an optimal magnetic field compensation. (d) Low n_l state, with an optimal compensation. On each picture, the black dot is the fitted center position of the beam for the current excitation wavelength and the white dot is the center position for the other wavelength, with the same magnetic field compensation. Without compensation, the n_l state is less deflected than the n_h state as expected from eq. (3.4). With compensation, the beam hits the same position on the MCP for n_h and n_l, resulting from the compensation procedure.

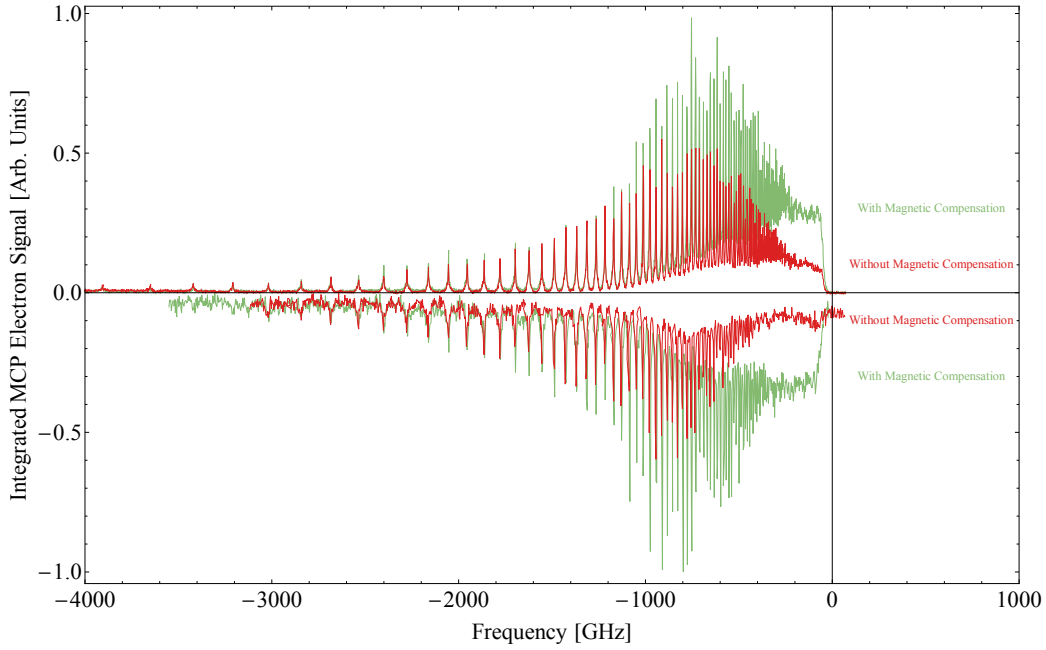

Figure 16: Rydberg spectra measured without (red curves) and with (green curves) magnetic field compensation, with every other parameters identical. Top: Spectra obtained by integration of the time trace. Bottom: Spectra obtained by integrating over the MCP screen, with measured values multiplied by -1 for display reasons.

3.4 Measurement of Rydberg spectra with magnetic field compensation

In order to quantify the quality of the measurements with the magnetic field compensation, a spectrum of the He Rydberg atoms was measured using the time trace of the MCP signal and compared to the same spectrum without magnetic field compensation (Fig. 16, top). We observe a significant improvement of the measured signal, especially in the high frequencies region, corresponding to the high n state numbers. At the highest frequencies, we can see that the ionization limit is much sharper with compensation, which is closer to the theoretical situation. This matches the expectations: since higher n states are more sensible to the magnetic field, the deviation of the electron beam is bigger than the size of the MCP and a part of the beam misses the MCP and is not detected, decreasing the measurement signal. These spectra are another confirmation that we could successfully compensate the ambient parasitic magnetic fields in the lab and thus improve the measurements quality.

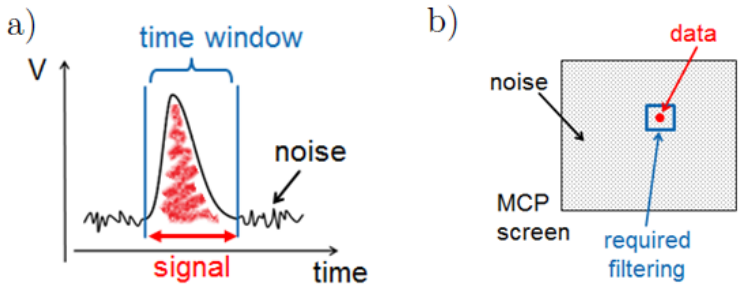

Figure 17: Simplified principle of the two different measurement shemes. a) Time-resolved measurement. The noise is filtered out from the integrated signal using a time window. b) Signal from the MCP screen. A spatial filtering would be required to filter out the noise from the whole screen.

In a second time, the same measurement was done by measuring the integrated signal on the MCP screen instead of the time trace as usual (Fig. 16, bottom). This implies a much lower signal to noise ratio, since the noise background, that can be suppressed by a time window from the time trace, is included when integrating over the whole MCP screen, see Fig. 17. We would need a spatial filter to reduce the noise. However, the quality of the spectrum is similar to the first case, especially when the magnetic compensation is used. This means that future experiments can rely on the imaging as a measurement tool.

3.5 Application: Study of the beam focalization

We want to illustrate further the advantages of the magnetic field compensation on the experiment. For that purpose, we choose to study the focalization of the electron beam.

The third zone of the experiment, where atoms are ionized, contains three electrodes [1]. So far, we applied a potential of 1.2kV between electrodes 3 and 4 to ionize Rydberg atoms and produce the electron beam. But there are actually 3 more electrodes in an Einzellens configuration that can be compared to a classical lens used for light. We bias electrode 6 with a voltage to study the effect on the beam focalization. Tuning the voltage in this electrode has the effect of changing the focal length of the ion lens. The electron beam width was measured for different voltages in electrode 6, also referred to as ion electrode, see Fig. 18.

For small voltages, a lorentzian fit was used for the beam shape. The width of the beam is given by the FWHM of the fitted lorentzian function. However the shape of the beam is anisotropic in x and y directions, so one

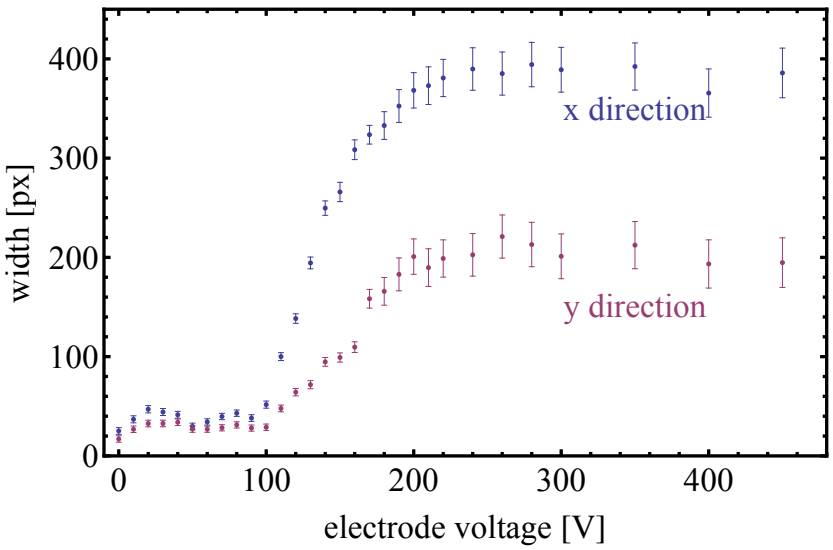

Figure 18: Width of the beam on the MCP screen depending on the voltage of the ion electrode. The beam is not circle-shaped: the blue dots are widths in the x direction and the purple dots widths in the y direction.

fit was used for each direction, giving two values for the width (Fig. 18). For higher voltages, defocalization makes the beam become wider and the lorentzian fit is no longer valid. In this case, we manually select a line $y = const.$, and find the two pixels where intensity is half the maximum intensity along the line. This gives a width in x direction ; the same is done for y direction. Of course, in the latter case errors bars are significantly higher than with the lorentzian fit.

There is still a need for proper theoretical simulations to fully understand the results from Fig. 18 but we can already suggest an explanation for some of the features we observe. First, when we start increasing the electrode voltage, the beam width slightly increases and we then observe a focalization for voltages around 50V. This is expected because increasing the electrode voltage is equivalent to modifying the focal lens of the ion lens. With zero voltage, we start from a lens focused on infinity. Then the focal length decreases as the electrode voltage increases, as the beam width is reduced by this progressive focalization. The beam width is minimal when the voltage is such that the focal length is equal to the distance between the ion lens and the MCP screen, i.e. when the beam is properly focalized on the MCP. Here, although the beam width is comparable for a voltage of 50V and zero voltage, the intensity of the peak is much higher in the first case, where the beam is focalized. If the electrode voltage is increased further, the focal

length becomes smaller and we loose the focalization on the MCP screen. The beam width increases again, first slightly as we observe for voltages between 60V and 100V, then strongly after $V = 100$V. This could be due to the fact that when the focal length is shorter than the distance to the MCP, there is a point where the electron beam will be very narrow. Unlike for light, electrons repel each other, such that the beam after this point will be much broader than in the analogy with light we used so far. Also, the lens focal length does not depend linearly on the voltage applied in the ion electrode. Finally, from voltages around 200-250V, the beam width becomes constant. This is the limit of the electrodes hole size. The beam width at the last electrode is such that some of the electron will hit the electrode, such that we cannot observe a wider beam on the MCP. Instead, we loose a part of the signal and get smaller peak intensities.

It is important to realize that this study would not have been possible without the magnetic field compensation developed earlier. Indeed, considering the beam deflection, when the beams becomes wider with increased voltage it will start to hit the extremity of the MCP and finally only a part of the beam is visible on the screen, making any measurement of its width impossible. This study thus illustrates that the quality of measurements can be increased thanks to the magnetic field compensation, especially regarding the imaging of the beam.

Conclusion

An ensemble of coils was designed and built in order to achieve an active compensation of the ambient magnetic field in the lab. Those coils were characterized, and using the current supply device built previously [2], the magnetic field inside the coils can be tuned.

However, the accessible range of magnetic field that can be generated with the setup is relatively limited. As such, we are not able to tune the six sensor signals at the same time, and currently coil Z2 is in practice not used. As we have seen, this is on the one hand because of the current limitation in coils because of the op-amps supply voltage. This problem has yet been addressed by replacing op-amps but the coils current limit was not tested with those new op-amps. On the other hand, the way current in coils is driven as a function of the measured sensors signals is still not optimal. A solution was suggested in section 2.3 to improve this, and was partially tested with old op-amps, where it was indeed more efficient, but could not be tested with the new op-amps.

Nevertheless, we have proven that the initial goal was successfully fulfilled, since we defined a procedure that allows to annihilate the electron beam deviation observed at the MCP, whatever the n state the Rydberg atoms are prepared in. This enables an increased measurement precision, for example of the spectrum of our Rydberg atoms, and more importantly opened a range of measurement using the imaging of the Rydberg electron beam. The study of the beam focalization is a good example of a measurement that was not possible without a magnetic field compensation, and we believe that being able to spatially resolve the electron beam is a useful asset for the Rydberg experiment.

Acknowledgments

I would like to give my sincere thanks to Tobias Thiele for his availability, his useful advices and his precious contribution to guide my work. It was a pleasure to work with him. Many thanks to Seppi for his ingenious solution that enabled the winding of approximately 3km of wire with relative ease. The POM coils structures were built by the ETH Physics Workshop. I want to thank Florian Lüthi who took the time to introduce me to his previous work and helped me fix the amplifier circuit more than once. Stefan Filipp was of a great help for the LabView program and for his precious advice and remarks. I'm also grateful to Hansjürg Schmutz for identifying the cause in the amplifier circuit for the voltage limitation in coils. Last but not least, I want to thank of course Prof. Andreas Wallraff for giving me the opportunity to work in the Quantum Device Lab. This was an interesting project to work on and I appreciated the atmosphere in the group and the work environment.

References

[1] T. Thiele, S. Filipp, J. A. Agner, H. Schmutz, J. Deiglmayr, M. Stammeier, P. Allmendinger, F. Merkt and A. Wallraff, Manipulating Rydberg atoms close to surfaces at cryogenic temperatures, Physical Review A **90** 013414 (2014).

[2] F. Lüthi, Active Magnetic Field Compensation, Semester Thesis, ETH Zürich/Quantum Device Lab, 2014.

[3] M. A. Azpurua, A semi-analytical method for the design of coils systems for homogeneous magneto-static field generation, Progress In Electromagnetics Research B **37** 171-189 (2012).

[4] K. Kuns, Calculation of Magnetic Field Inside Plasma Chamber, online: http://plasmalab.pbwiki.com/f/bfield.pdf, 2007.

[5] L. Gerster, Metastable Helium source, Semester Thesis, ETH Zürich/Quantum Device Lab, 2014.

[6] M. Melchner, Collimation of metastable 2^3S_1 helium atoms using laser cooling techniques, Semester Thesis, ETH Zürich/Quantum Device Lab, 2014.

[7] Texas Instruments, OPA445 Operational Amplifier Datasheet, online: http://www.ti.com.cn/cn/lit/ds/symlink/opa445.pdf

Appendix

A Magnetic field density generated by a rectangular coil

We want to determine the magnetic field density generated in every point of space by the square coils pair with main axis x (see Fig. 1). The coils have a dimension $l \times h$ and their center position is $(\pm l/2, 0, 0)$. In the following we note $a = l/2$, $b = h/2$ and $c = w/2$. We first look for the field created by a single coil, e.g. the one which center is $(a, 0, 0)$. Starting from the general expression of Biot-Savart's law:

$$\vec{B}(\vec{r}) = \frac{\mu_0}{4\pi} \int_V \frac{\vec{J}(\vec{r'}) \times (\vec{r} - \vec{r'})}{|\vec{r} - \vec{r'}|^3} d\vec{r'} \tag{A.1}$$

Where $\vec{J}(\vec{r'})$ is the current density at position $\vec{r'}$ and where integration volume V is the whole space. In the system we consider, the current density is non-zero only in the coil wire. The link between current density $\vec{J}$ and current flowing through the coil I is:

$$NI.d\vec{l} = \iint_S \vec{J}.d\vec{S} \tag{A.2}$$

Where S is the section of the coil wire and N the number of windings. We can transform the integral over space in (A.1) into a path integral:

$$\vec{B}(\vec{r}) = \frac{\mu_0}{4\pi} NI \oint_\gamma \frac{d\vec{l} \times (\vec{r} - \vec{r'})}{|\vec{r} - \vec{r'}|^3} \tag{A.3}$$

The path is the coil itself. This closed integral can be decomposed in four integrals running over each side of the coil:

$$\vec{B}(\vec{r}) = \vec{B_1}(\vec{r}) + \vec{B_2}(\vec{r}) + \vec{B_3}(\vec{r}) + \vec{B_4}(\vec{r}) \tag{A.4}$$

For the rectangular coil of interest, the path-element takes two different forms, whether we consider a $y = const.$ or a $z = cst$ segment. We consider first the $y = b$ segment, which creates the field B_1. Only dz' is non-zero. The tensor product reduces to:

$$d\vec{l} \times \vec{r} = \begin{pmatrix} -(y - y')\ dz' \\ (x - x')\ dz' \\ 0 \end{pmatrix}$$

Thus the x component of the magnetic field density created by this side, noted $B_{1,x}$ is:

$$B_{1,x}(x,y,z) = \frac{\mu_0}{4\pi} NI \int_{-c}^{c} \frac{-(y-b)}{((x-a)^2+(y-b)^2+(z-z')^2)^{3/2}}\, dz' \tag{A.5}$$

This can be solved analytically:

$$B_{1,x}(x,y,z) = \frac{\mu_0}{4\pi} NI \left[\frac{(y-b)(z-z')}{(x-a)^2+(y-b)^2} . \frac{1}{\sqrt{(x-a)^2+(y-b)^2+(z-z')^2}} \right]_{-c}^{c} \tag{A.6}$$

To simplify the expression, we introduce the following notation:

$$\mathscr{I}_b(c) = \frac{(y-b)(z-c)}{(x-a)^2+(y-b)^2} \frac{1}{\sqrt{(x-a)^2+(y-b)^2+(z-c)^2}} \tag{A.7}$$

Where the index b refers to the position of the segment considered and the variable c refers to an extremity of the segment. Keep in mind that $\mathscr{I}_b(c)$ still depends on x, y, z and on a. We get:

$$B_{1,x}(x,y,z) = \frac{\mu_0}{4\pi} NI \left(\mathscr{I}_b(c) - \mathscr{I}_b(-c) \right) \tag{A.8}$$

Similarly, the function $\mathscr{I}$ allows us to write directly the contribution $B_{3,x}$ due to the second segment parallel to the y axis, $y = -b$:

$$B_{3,x}(x,y,z) = \frac{\mu_0}{4\pi} NI \left(\mathscr{I}_{-b}(-c) - \mathscr{I}_{-b}(c) \right) \tag{A.9}$$

In this case, whereas the path-element is the same, the integral has to be computed from c to $-c$, hence the minus sign in $B_{3,x}$ compared with $B_{1,x}$. It is clear from (A.3) that every contribution to the magnetic field created by any segment parallel to one of the axes will have a similar form to (A.5). We introduce three other functions similiar to $\mathscr{I}_b(c)$:

$$\mathscr{J}_c(b) = \frac{(y-b)(z-c)}{(x-a)^2+(z-c)^2} \frac{1}{\sqrt{(x-a)^2+(y-b)^2+(z-c)^2}} \tag{A.10}$$

$$\mathscr{K}_b(c) = -\frac{(x-a)(z-c)}{(x-a)^2+(y-b)^2} \frac{1}{\sqrt{(x-a)^2+(y-b)^2+(z-c)^2}} \tag{A.11}$$

$$\mathscr{L}_c(b) = -\frac{(x-a)(y-b)}{(x-a)^2+(z-c)^2} \frac{1}{\sqrt{(x-a)^2+(y-b)^2+(z-c)^2}} \tag{A.12}$$

We finally have:

$$B_x(x,y,z) = \frac{\mu_0}{4\pi} NI \left(\mathscr{I}_b(c) - \mathscr{I}_b(-c) - \mathscr{I}_{-b}(c) + \mathscr{I}_{-b}(-c) \right.$$
$$\left. + \mathscr{J}_c(b) - \mathscr{J}_c(-b) - \mathscr{J}_{-c}(b) + \mathscr{J}_c(b)\right) \quad \text{(A.13)}$$

$$B_y(x,y,z) = \frac{\mu_0}{4\pi} NI \left(\mathscr{K}_b(c) - \mathscr{K}_b(-c) - \mathscr{K}_{-b}(c) + \mathscr{K}_{-b}(-c)\right) \quad \text{(A.14)}$$

$$B_z(x,y,z) = \frac{\mu_0}{4\pi} NI \left(\mathscr{L}_b(c) - \mathscr{L}_b(-c) - \mathscr{L}_{-b}(c) + \mathscr{L}_{-b}(-c)\right) \quad \text{(A.15)}$$

The expression of the magnetic field density $\vec{B}_X$ generated by the coil pair is obtained through the sum of the field created by each coil:

$$\vec{B}_X(\vec{r}) = \vec{B}_{X1}(\vec{r}, N_1, I_1) + \vec{B}_{X2}(\vec{r}, N_2, I_2) \quad \text{(A.16)}$$

where coil 1 (resp. 2) generates fields $\vec{B}_{X1(2)}$. The expression for $\vec{B}_{X2}$ is simply obtained by changing a to $-a$ in (A.13), (A.14) and (A.15). Winding numbers N_1, N_2 and intensities I_1, I_2 where used as parameters to emphasize that both coils can have a different winding number, and more importantly, different intensities flowing through them.

B LabView program and interface

In this section, we explain how to use the LabView program controlling the currents sent to the coils, and give a few details about the changes that were introduced to the version of the program described in [2].

The magnetic field control program is included in the main logger program of the Rydberg experiment. It can be found in the tab "BField" as shown Fig. 19. First thing that needs to be checked before running the program: AIP and AOP parameters should be the same as those visible Fig. 19, otherwise the program won't run and and error is returned. The path to the file were the logs are saved should also be correctly given. Finally, the time step between two readouts of the sensors values and correction to the coils currents can be changed via parameter "Read Interval BField", however its value cannot be less than 500ms.

Once the initialization parameter are set, the program can be started. As long as the "Output Creator" switch is turned off, no current will be sent to the coils and the program will just display the ambient magnetic field measured by sensors. "Output Creator" switch has to be turned on to start sending current to the coils. "Direction Corrections" controls enable to select which sensors signal should be controlled. For example, if the first value is 1, currents in coils will be adjusted so that signal X1 goes to the first "Offset"

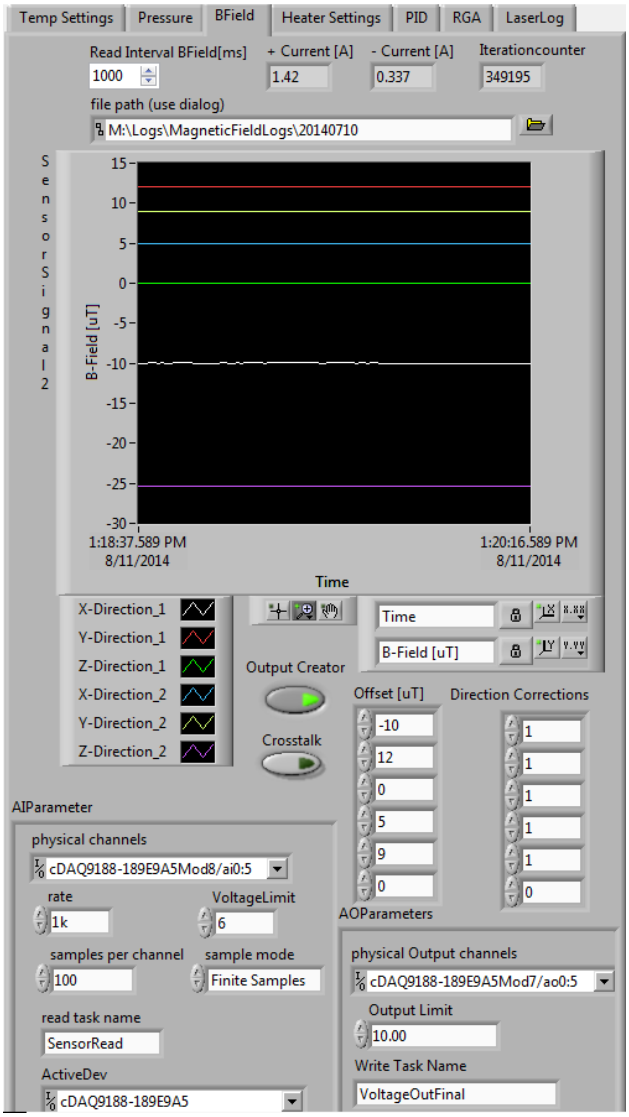

Figure 19: Front panel of the magnetic field control program, included in the main logger program.

control value. "Offset" thus allow to tune the magnetic field created by coils. If the "Direction Corrections" value is 0, then the corresponding signal is not taken into accounts to determine currents to send in coils. In Fig. 19, only first 5 signals are taken into account and we can see that the corresponding measured signals are adjusted to their respective desired offsets. Only signal Z2 is not adjusted to its offset. Finally, the "Crosstalk" switch allow to choose how currents are determined from measured signals. If the switch is off, the currents are driven as described in [2], i.e one signal drives one coil.

If the switch is on, currents are determined by inverted equation 2.1. Pay attention that this version does not work perfectly currently. It might be wiser to stay with "Crosstalk" switched off, or at least have a look at the implementation and the crosstalk matrix values used before turning it on.

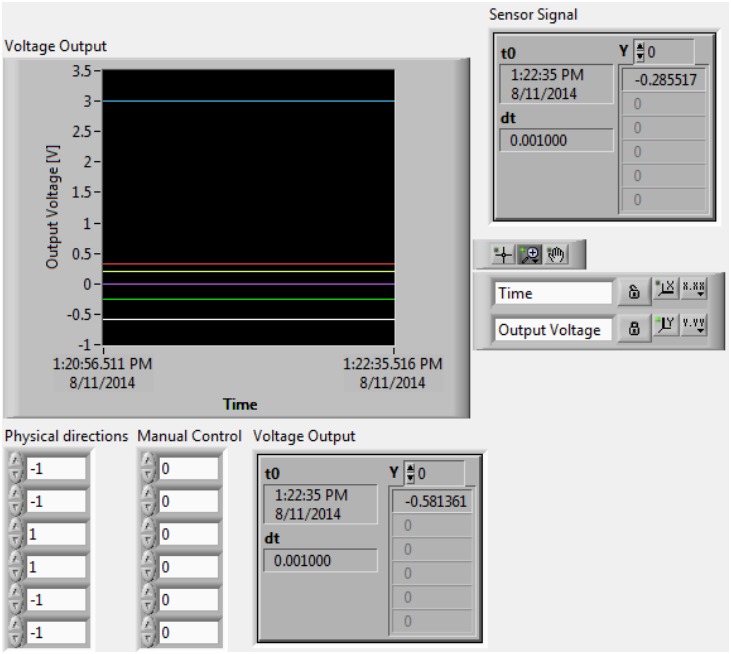

Figure 20: Front panel showing the voltages sent to coils, also part of the logger front panel.

More information can be found on the front panel of the main logger, below the two main pressure and temperature signals. Those supplementary information, that can prove useful, are shown Fig. 20. First, voltages sent to each coils are displayed. Second, notice "Physical directions" and "Manual control" controls. "Manual control" allows to send a constant voltage to any coils. The given value has to be given in V and correspond to values that are displayed above. Remember conversion factor 4/10 between current in coil and input voltage. It is disadvised to sent some constant voltage if the corresponding "Direction Corrections" is 1, i.e if feedback is running for the considered coil. Finally, "Physical directions" refers to the relation between sensor axes and our choice of axes (see Fig. 1). If sensors are not moved, "Physical directions" must not be changed. Otherwise, when sensors are moved, their axes should always match our conventional x, y, z axes, but a ± 1 factor may has to be adjusted. This is what "Physical directions" are for.

Fig. 21 shows the part of the VI corresponding to the magnetic field control program as it was included in the main logger VI. It is very similar to

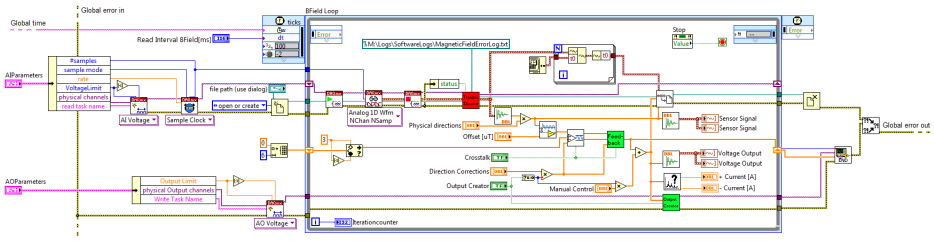

Figure 21: Diagram of the magnetic field control program, as it was included in the main logger VI.

the one from [2]. Changes are due for example to adding a few options, such as "Output Creator", "Manual control", "Crosstalk", etc. Also, the program was made cleaner and safer. "Offsetter" subVI was cleaned, a "Signal preparation" subVI was added to allow better control of currents with "Direction Corrections", especially going back to zero voltage when we wish to stop feedback in a given coil. The absolute value of input voltages can never higher than 3V, even though the current limit should correspond to values around maximum 2V with new op-amps. Voltage variations are limited to 0.5V per time step to avoid problems in the electronic circuit. This also holds true when the program is turned off. Important, voltages displayed on front panel now always correspond to voltages sent to the input card. Do not hesitate to take a look at the subVIs to better understand the subtleties if needed.

Eidgenössische Technische Hochschule Zürich
Swiss Federal Institute of Technology Zurich

Declaration of originality

The signed declaration of originality is a component of every semester paper, Bachelor's thesis, Master's thesis and any other degree paper undertaken during the course of studies, including the respective electronic versions.

Lecturers may also require a declaration of originality for other written papers compiled for their courses.

I hereby confirm that I am the sole author of the written work here enclosed and that I have compiled it in my own words. Parts excepted are corrections of form and content by the supervisor.

Title of work (in block letters):

Realization of an active magnetic field compensation

Authored by (in block letters):
For papers written by groups the names of all authors are required.

Name(s):	**First name(s):**
Goblot	Valentin

With my signature I confirm that

- I have committed none of the forms of plagiarism described in the 'Citation etiquette' information sheet.
- I have documented all methods, data and processes truthfully.
- I have not manipulated any data.
- I have mentioned all persons who were significant facilitators of the work.

I am aware that the work may be screened electronically for plagiarism.

Place, date	**Signature(s)**
Zurich, 10th September 2014	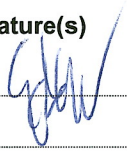

For papers written by groups the names of all authors are required. Their signatures collectively guarantee the entire content of the written paper.